Measured Potential Profile in a Quantum Anomalous Hall System Suggests Bulk-Dominated Current Flow

Ilan T. Rosen, Molly P. Andersen, Linsey K. Rodenbach, Lixuan Tai, Peng Zhang, Kang L. Wang, M. A. Kastner, and David Goldhaber-Gordon

Phys. Rev. Lett. **129**, 246602 — Published 9 December 2022

DOI: 10.1103/PhysRevLett.129.246602

Measured potential profile in a quantum anomalous Hall system suggests bulk-dominated current flow

Ilan T. Rosen,[1,2,*] Molly P. Andersen,[3,2] Linsey K. Rodenbach,[4,2] Lixuan Tai,[5] Peng Zhang,[5] Kang L. Wang,[5] M. A. Kastner,[4,2,6] and David Goldhaber-Gordon[4,2,†]

[1] *Department of Applied Physics, Stanford University, Stanford, California 94305, USA*
[2] *Stanford Institute for Materials and Energy Sciences, SLAC National Accelerator Laboratory, Menlo Park, California 94025, USA*
[3] *Department of Materials Science and Engineering, Stanford University, Stanford, California 94305, USA*
[4] *Department of Physics, Stanford University, Stanford, California 94305, USA*
[5] *Department of Electrical Engineering, University of California, Los Angeles, California 90095, USA*
[6] *Department of Physics, Massachusetts Institute of Technology, Cambridge, Massachusetts 02139, USA*

Ideally, quantum anomalous Hall systems should display zero longitudinal resistance. Yet in experimental quantum anomalous Hall systems elevated temperature can make the longitudinal resistance finite, indicating dissipative flow of electrons. Here, we show that the measured potentials at multiple locations within a device at elevated temperature are well-described by solution of Laplace's equation, assuming spatially-uniform conductivity, suggesting non-equilibrium current flows through the two-dimensional bulk. Extrapolation suggests that at even lower temperatures current may still flow primarily through the bulk rather than, as had been assumed, through edge modes. An argument for bulk current flow previously applied to quantum Hall systems supports this picture.

The quantum anomalous Hall (QAH) effect ideally features longitudinal resistivity ρ_{xx} that vanishes as the Hall resistivity ρ_{xy} approaches $\pm h/e^2$. Such quantized Hall resistivity has been confirmed with high precision in magnetically-doped films of the topological insulator $(\mathrm{Bi,Sb})_2\mathrm{Te}_3$ at zero or low magnetic field [1–6]. The onset of dissipation, where ρ_{xx} becomes finite and ρ_{xy} departs from h/e^2, may be induced through increasing the temperature, increasing the source-drain bias, or electrostatic gating. Understanding the dissipative state is crucial for quantifying and improving material quality, with the goal of engineering materials in which the anomalous Hall effect is quantized at higher temperatures.

The QAH system has been theoretically shown to host a chiral edge mode (CEM) [7, 8] associated with the system's nonzero Chern number. Scanning measurements of local microwave impedance appear to show conducting edge modes [9]. The general understanding in the field has been that non-equilibrium current—current flowing in response to applied source-drain bias, as distinct from the persistent circulating current—flows through the CEM [1–6, 9–12]. This understanding originates in early pictures of the quantum Hall (QH) system [13, 14]. Yet a recent study of transport in QAH Hall bar and Corbino geometries at high bias identified that dissipation occurs through the two-dimensional bulk, requiring at least some bulk current flow in dissipative regimes [15]. That study suggests the need for further inquiry into the conditions under which current flows in the bulk versus through the edges, and whether dissipation in the bulk is spatially uniform or is higher in particular areas of devices.

In this work, we measure the longitudinal voltage at various points along the edge of a current-biased Hall bar in the QAH state at the onset of dissipation. We find that the longitudinal electric field is not uniform, but rather varies monotonically along each edge of the Hall bar. We find that, when dissipation is induced by increased temperature, the spatial profile of the measured potential in the QAH system nearly perfectly matches numerical simulations of Laplace's equation that assume spatially uniform longitudinal and Hall conductivity within the device geometry. Mirroring arguments borrowed from the QH literature [16–19], we deduce that the source-drain bias manifests primarily as a transverse electric field that drives current through the two-dimensional bulk. That this holds down to $\rho_{xx} \approx 0.01 h/e^2$ (the lowest we can probe with small enough uncertainties) raises the possibility that even in the dissipationless regime, non-equilibrium current in the QAH system may flow through the bulk of the material and not, as has been generally assumed, through chiral edge modes.

METHODS

Here we study low-frequency electronic transport in a Hall bar fabricated from a 6 nm film of $(\mathrm{Bi}_x\,\mathrm{Sb}_{1-x})_2\mathrm{Te}_3$, with layers near the top and bottom heavily doped with Cr. The fabrication process, described in Ref. [15], in-

* Current address: Research Laboratory of Electronics, Massachusetts Institute of Technology, Cambridge, MA 02139, USA; itrosen@mit.edu
† goldhaber-gordon@stanford.edu

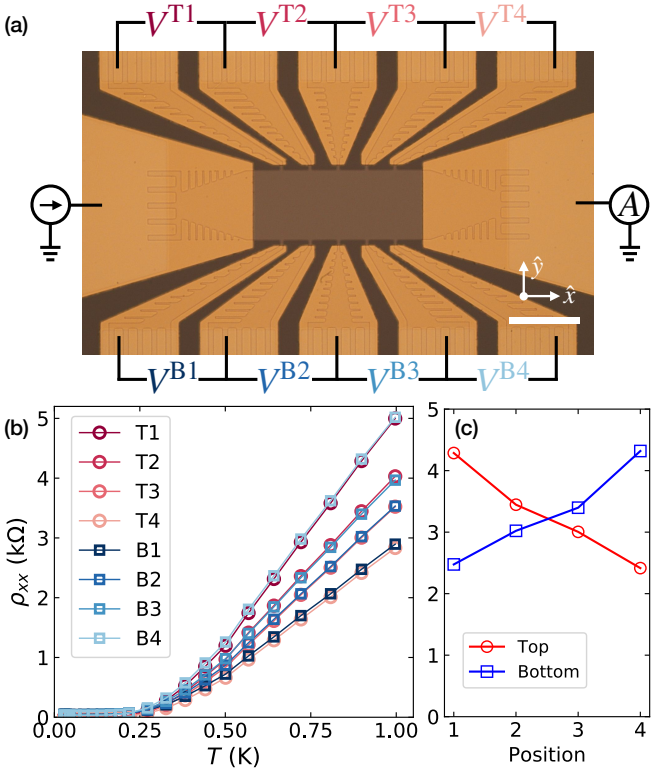

FIG. 1. (a) Optical micrograph of the Hall bar prior to top gate metal deposition. Current injection at the source terminal (left) and current measurement at the drain terminal (right) are indicated, along with the eight longitudinal voltage measurements $V_{xx}^{\alpha i}$ enabled by the ten voltage taps. Coordinate axes are indicated. Scale bar, 100 μm. (b) The apparent resistivities as a function of temperature at the optimum gate voltage. (c) Apparent resistivity shown as a function of position on the top and bottom edges of the Hall bar at 898 mK.

cludes an electrostatic top gate with an alumina dielectric to control the Fermi level. The Hall bar features five voltage taps spaced evenly along the top edge and five more along the bottom edge, so that the longitudinal voltage drop can be measured across four consecutive segments along each edge (Fig. 1(a)). We define the apparent differential resistivities

$$\rho_{xx}^{\alpha i} = \frac{W}{L}\frac{dV^{\alpha i}}{dI}, \tag{1}$$

where $\alpha = \mathrm{T}, \mathrm{B}$ indexes the top and bottom edges of the Hall bar, $i = 1, 2, 3, 4$ indexes the four measurement segments across the Hall bar from left to right, $W = 100$ μm is the width of the Hall bar, and $L = 40$ μm is the length between voltage taps for each measurement segment. A 5 nA ac current bias is applied to the source terminal at the left edge of the device, and a dc current bias is added in measurements where indicated. The differential longitudinal voltages $dV^{\alpha i}$ and the ac bias current dI are amplified and measured simultaneously with separate lock-in amplifiers [20].

Measurements are made in a dilution refrigerator with a base temperature of 28 mK at zero external field after magnetizing the film with an out-of-plane field of 0.4 T. Dissipation is induced in three ways: (1) by increasing the temperature of the system, (2) by applying nonzero dc bias, and (3) by tuning the gate voltage away from its optimal value. The temperature is increased using a heater on the mixing chamber stage of the refrigerator, and is measured by a thermometer also on the mixing chamber stage. Electronic wiring is thermalized to the mixing chamber temperature through filters attached to the mixing chamber stage so that when the mixing chamber stage is heated, the sample's electron temperature and lattice temperature should both track the mixing chamber temperature. In the Supplemental Material, we discuss additional data taken while heating in a manner designed to preferentially heat the electronic system or the lattice.

RESULTS

At base temperature and with magnetization directed vertically upward (henceforth referred to as positive magnetization), the Hall resistance is quantized (zero longitudinal resistance and Hall resistance $-h/e^2$), within the precision of the measurement over a wide range of gate voltages V_g. The optimum gate voltage, that which minimizes the longitudinal resistivity at an elevated temperature, is -1.18 V. Here, the conductivity of the device versus temperature is well-fit by Arrhenius activation with a temperature scale of 1.40 K [20]. All measurements, aside from those where the gate voltage is explicitly varied, are taken at $V_g = -1$ V.

Fig. 1(b) shows $\rho_{xx}^{\alpha i}$ as a function of temperature. At a given temperature, the apparent resistivity is not constant throughout the device, but follows a pattern that is clarified in Fig. 1(c) by plotting the resistivities as a function of position. The apparent resistivity decreases (increases) monotonically moving rightwards across the top (bottom) edge of the device. The apparent resistivities on opposite ends of opposite edges are approximately equal, so that the largest are $\rho_{xx}^{\mathrm{T1,B4}}$.

This pattern is reminiscent of the classical Hall effect, where the electric potential ϕ satisfies Laplace's equation $\nabla^2\phi = 0$ subject to Dirichlet boundary conditions at the source and drain contacts and the condition

$$\frac{d\phi}{dy} = \frac{\sigma_{xy}}{\sigma_{xx}}\frac{d\phi}{dx} \tag{2}$$

at edges of the device without contacts (the top and bottom edges of the Hall bar) [21]. The latter conditions are a statement of current continuity at the device edges. To compare our measurements with solutions of Laplace's equation, we numerically solve Laplace's equation in the specific geometry of our Hall bar for a variety of values

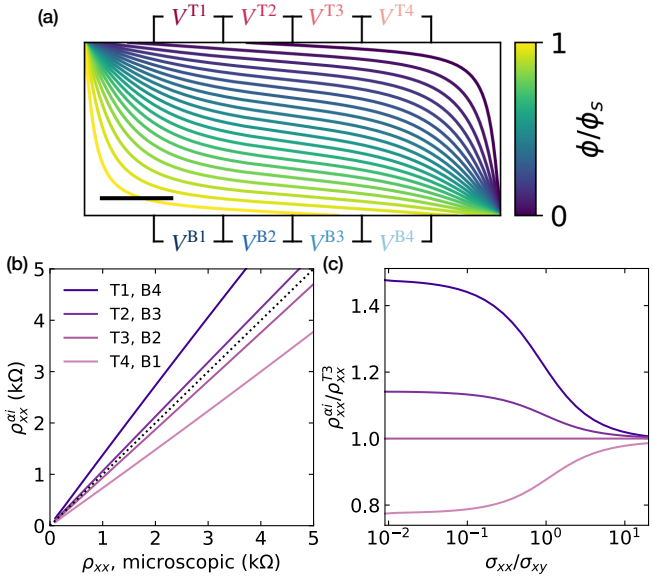

FIG. 2. (a) Contour plot of equipotentials, normalized to the source potential ϕ_s, in the Hall bar simulated at $\sigma_{xx}/\sigma_{xy} = 0.05$, with positive magnetization. The electric field is concentrated near the top left and bottom right corners. Scale bar, 40 μm. (b) Simulated apparent resistivities $\rho_{xx}^{\alpha i}$ as a function of the spatially-homogeneous microscopic resistivity of the material. The dotted line with a slope of 1 is included for reference. (c) The ratio of simulated resistivities $\rho_{xx}^{\alpha i}/\rho_{xx}^{T3}$.

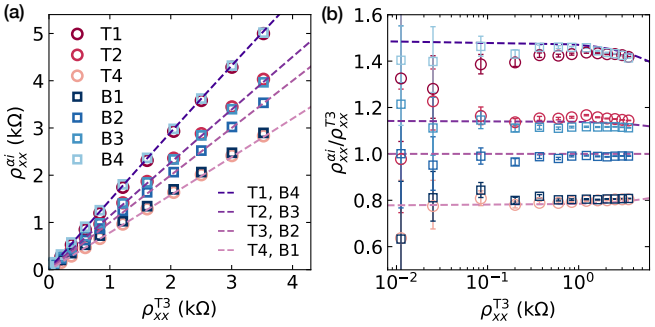

FIG. 3. (a) The apparent resistivity at multiple locations and multiple temperatures (data from Fig. 1(b)), plotted parametrically versus measurement T3 at the same temperature. The simulated behavior (Fig. 2(b)) is shown by the dashed violet lines. (b) The ratio of measured apparent resistivities $\rho_{xx}^{\alpha i}/\rho_{xx}^{T3}$, shown as a function of measured ρ_{xx}^{T3}. Simulated behavior (Fig. 2(c)) is shown by the dashed violet lines. Data in (b) are corrected for finite input impedance of our voltage preamplifiers. The corrections and error budget are described in the Supplemental Material.

of the parameter σ_{xx}/σ_{xy}. An example result is shown in Fig. 2(a), demonstrating concentration of the electric field $\mathbf{E} = \nabla\phi$ in the top left and bottom right corners.

The simulated apparent resistivities, shown in Fig. 2(b) as a function of the spatially-homogeneous microscopic resistivity [20], reproduce several key features of our measurements. For nonzero σ_{xx} and σ_{xy}, resistivities measured at different locations are unequal. The apparent resistivity along the top (bottom) edge increases monotonically nearer to the left (right) corner. Centrosymmetry is intact: the apparent resistivities on opposite sides of opposite edges are equal.

We next quantitatively compare the simulations to the measurements. The microscopic resistivity cannot be directly determined from the measurements. We therefore parametrically plot $\rho_{xx}^{\alpha i}$ versus its value at one arbitrarily-chosen location ρ_{xx}^{T3}, providing a parameter-free measure of the spatial variation of the electric field. The data from Fig. 1(b) are shown in this manner in Fig. 3(a). The concurrence between simulations and measurements is striking, and, as emphasized in Fig. 3(b), holds in the low-dissipation limit to $\rho_{xx} \sim 200\ \Omega \approx 0.01h/e^2$, below which measurement errors become so large as to prevent meaningful comparison to our model.

When the magnetization of the film is reversed, switching the sign of the Hall conductance, the aforementioned pattern reverses, so that $\rho_{xx}^{T4,\,B1}$ are highest. Measurements for negative magnetization are shown in the Supplemental Material, and are also in good agreement with simulations.

DISCUSSION

Voltage contacts measure the local electrochemical potential, which in this experiment is the sum of the chemical potential of the CEM and the electrostatic potential. Our experiment shows that the electrochemical potential along the edge of a dissipative-regime quantum anomalous Hall system satisfies Laplace's equation in two dimensions. From this, we will next deduce that there is a transverse electric field E_y across the device and, in turn, that current flows through the bulk.

Just as voltage contacts measure local electrochemical potential, applied voltage imposes an electrochemical potential difference between source and drain. The way the electrochemical potential falls across the sample may in general be split between electrostatic and chemical potential gradients, the latter of which drives current through the CEM [13]. Let us consider whether one of those components is dominant in our measurements, or if both play roles. The electrostatic portion should satisfy Laplace's equation (the electrostatic potential should always satisfy Poisson's equation; that it should satisfy Laplace's equation follows from the assertion that Ohm's law $\mathbf{j} = \boldsymbol{\sigma}\mathbf{E}$ and conservation of charge $\nabla\mathbf{j} = 0$ hold [20]). In contrast, absent elaborate fine-tuning, models for dissipative-regime edge mode transport yield chemical potential profiles that *do not* satisfy Laplace's equation in two dimensions, as we demonstrate in the Supplemental Material. As Laplace's equation is linear, the sum of electrostatic and electrochemical po-

tentials thus should not be expected to satisfy Laplace's equation unless the electrochemical component is negligible. Our experimental finding that electrochemical potential *does* satisfy Laplace's equation along the sample edge then strongly suggests that the source-drain bias primarily drives an electrostatic potential gradient E_y throughout the bulk, not a chemical potential gradient across the CEM. That the potential profile is electrostatic could not have been concluded simply based on measuring current from source to drain: net current can flow from source to drain through the CEM in response to a chemical potential difference, even with no electric field anywhere in the sample [13].

Next, we consider the relationship between the electrostatic potential and the chemical potential throughout the bulk, noting that whereas electrostatic potential is uniquely defined (up to a constant) at every location in space, the chemical potential of the bulk does not necessarily equilibrate with that of the CEM. When the electrostatic potential in a small area of the bulk changes, charge enters the region according to its geometric capacitance, in turn proportionally modifying the chemical potential. This relationship may be represented as

$$\frac{\Delta\mu(x,y)}{e} = \frac{C_g}{C_q}\Delta\phi(x,y), \tag{3}$$

where $\Delta\mu$ and $\Delta\phi$ are the changes to the chemical and electrostatic potentials from the source-drain bias, respectively, C_g is the 2D bulk's geometric capacitance per unit area, and C_q is the 2D bulk's quantum capacitance per unit area, which here is determined by the density of localized states within the gap between the conducting surface state bands. In our device, C_g is dominated by the gate capacitance. We place an upper bound on C_g/C_q as follows: at base temperature, we observe a well-quantized QAH effect in this device across a gate voltage range of 6 V. Since the bulk conduction is small in this range, this gate voltage swing cannot change the chemical potential by more than the intrinsic gap, which has been measured in similar materials to be roughly 30 meV [22, 23] (this is a conservative upper bound; note that the aforementioned transport gap $k_B \times 1.40$ K $= 121$ μeV is orders of magnitude smaller). We thus bound $C_g/C_q \leq 1/200$. This calculation establishes that the electrochemical potential difference across the bulk of the device is almost entirely manifested as an electrostatic potential gradient $\nabla\phi$, not a chemical potential gradient $\nabla\mu$. We conclude that a source-drain bias is mostly manifested as an electrostatic potential difference, creating a transverse electric field within the device's 2D bulk.

Since there is a transverse electric field E_y, and we have $\sigma_{xx} \ll |\sigma_{xy}| \approx e^2/h$, it follows from Ohm's law $\mathbf{j} = \boldsymbol{\sigma}\mathbf{E}$ that the non-equilibrium current flows primarily through the two-dimensional bulk of the device. The ideal QAH system at zero temperature should have quantized conductivity $\sigma_{xx} = 0$, $\sigma_{xy} = \pm e^2/h$ (a consequence of the system's Chern number $C = \pm 1$, and derived via the Kubo formula [8]). The analysis technique presented in our present work requires measurable resistance. We have observed that the electrochemical potential continues to satisfy Laplace's equation as dissipation is reduced down to $\sigma_{xx} \sim 0.01h/e^2$ (Fig. 3(b)), the lowest we can access with acceptable resolution. Though we cannot make direct claims about the regime of even lower dissipation, this observation suggests that source-drain bias continues to manifest as a transverse electric field, and therefore that non-equilibrium current flows through the bulk, even in the limit $\sigma_{xx} \to 0$, where this current flows without dissipation and Hall resistance is precisely quantized.

We emphasize that we are here discussing the non-equilibrium portion of the the current, that is, the difference in total current with versus without a source-drain bias; even without bias a persistent current (from occupied states of the CEM) should also circulate around the edge of the device without contributing to a net source-drain current. Our experiment cannot discern through which two-dimensional states bulk currents flow—surface states or quantum well states derived from three-dimensional states—although we would predict the former. We also note that when $\sigma_{xx} = 0$, $\sigma_{xy} \neq 0$, in contrast to the dissipative regime we directly probe, resistances predicted by the Landauer-Büttiker formalism, based on the edge-current picture, are identical to those derived from Laplace's equation, even in nonlocal geometries [20].

Though our findings depart from the extant QAH literature, which generally presents dissipationless current flow as a circulating edge current, a strand of the QH literature has long recognized that the amount of non-equilibrium current flowing through the bulk versus the edge depends on the extent to which the source-drain bias manifests as an electrostatic or a chemical potential difference, respectively, and that the drop is often primarily electrostatic, implying bulk current flow [16–19, 24–29]. We present further comparison of the QAH and QH systems in the Supplemental Material.

Having so far focused on linear conductance, we now consider the QAH device subjected to a large current bias. The resulting large transverse electric field across the device induces dissipation and eventually breakdown of the QAH state [3, 4, 15]. Because the electric field is highest in two corners of the device (called the "hot spots" in this context) [27], we expect that the longitudinal conductivity becomes nonuniform, taking higher values near the hot spots. Solutions to Laplace's equation assuming uniform conductivity should thus no longer describe the potential throughout the device. In the Supplemental Material the apparent resistivities shown as a function of current bias (Fig. 4(a) of the main text) are compared to simulations of Laplace's equation. Indeed,

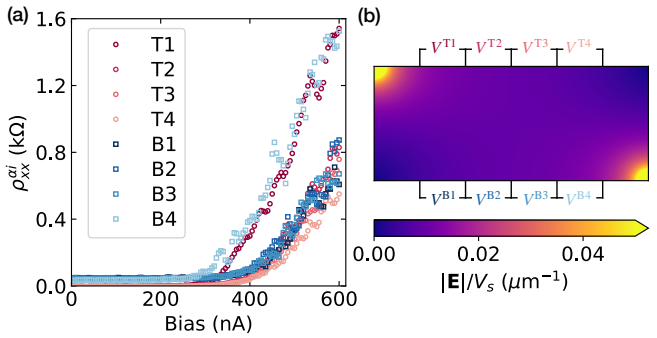

FIG. 4. (a) Resistivity as a function of applied dc bias at optimum gate voltage and $T \approx 28$ mK. (b) The electric field normalized to the source-drain bias, simulated using Laplace's equation with appropriate boundary conditions at edges of the device. For this simulation, conductivity is assumed to be uniform over the entire device. In fact, we know the conductivity is a strong function of electric field at high electric field, and since the simulation shows that electric field is non-uniform within the device, our model should be inaccurate at high current bias.

the data no longer match uniform-conductivity solutions to Laplace's equation. Near the hot spots (measurements T1 and B4), breakdown occurs at a lower bias and the resistivity increases more rapidly after breakdown. This effect is invariant to the sign of dc bias, but reverses, so that $\rho_{xx}^{\mathrm{T4,\ B1}}$ become highest, when the magnetization of the film is switched (thus switching which corners host the hot spots) [20].

CONCLUSION

We have here shown that the resistivity in Hall-geometry QAH devices in the dissipative regime varies as a function of where in the device the resistivity is measured. When the dissipation is induced by increased temperature, the spatial dependence of resistivity quantitatively matches solutions to Laplace's equation with finite and spatially-uniform longitudinal and Hall conductivities. This result is consistent with flow of non-equilibrium current primarily through the bulk, rather than the edges, of devices, which, we argue, should be expected in QAH devices. Our analysis extends that of Ref. [15], which showed that *dissipative* currents mostly flow through the bulk, but did not establish that the non-equilibrium current mostly flows through the bulk *even in the limit of low dissipation.*

The analysis presented in this work is limited to regimes with finite longitudinal conductivity, and we have discussed the dissipationless regime only by extrapolation from the low-dissipation limit. Using high-precision, high-input-impedance voltmeters [3] could allow similar analysis at even lower levels of dissipation, $\rho_{xx} \sim 10$ mΩ. Other measurements, such as scanning probe measurements of current flow or local potential, would enable study of the system's electronic behavior in the regime of vanishing longitudinal conductivity. Scanning impedance measurements under large current bias should also be able to detect local variation in the conductivity near the hot spots.

A recent study claimed the observation of chiral current flow in a modified Corbino device [30]. In the Supplemental Material, we reproduce with no free parameters the main features of the data using our simulations of Laplace's equation, which feature bulk-only current flow.

While preparing this manuscript, we became aware of work with similar conclusions being prepared by G. M. Ferguson *et al.* [31].

ACKNOWLEDGEMENTS

P. Z., L. T., and K. L. W. developed and grew the Cr-doped $(\mathrm{Bi}_x\,\mathrm{Sb}_{1-x})_2\mathrm{Te}_3$ film. I. T. R. and M. P. A. fabricated the devices. I. T. R. conducted low-frequency measurements and simulated the classical Hall effect. I. T. R., L. K. R., M. P. A., M. A. K., and D. G.-G. analyzed the data. I. T. R. wrote the manuscript with contributions from all authors.

We thank B. I. Halperin and R. B. Laughlin for enlightening discussions. I. T. R. acknowledges M. A. Zaman, upon whose code (available at `https://github.com/zaman13/poisson-solver-2D`) the simulations in this work are based, and enlightening discussions at the early stages of this work with G. M. Ferguson and K. C. Nowack. I. T. R., M. P. A., and L. K. R. were supported by the U.S. Department of Energy, Office of Science, Basic Energy Sciences, Materials Sciences and Engineering Division, under Contract DE-AC02-76SF00515. I. T. R. additionally acknowledges support from the ARCS foundation. P. Z., L. T., and K. L. W. were supported by the U.S. Army Research Office MURI program under Grants No. W911NF-16-1-0472. Infrastructure and cryostat support were funded in part by the Gordon and Betty Moore Foundation through Grant No. GBMF3429. We thank NF Corporation for providing low-noise, high-input-impedance voltage preamplifiers. We acknowledge measurement assistance from colleagues at the National Institute of Standards and Technology. Part of this work was performed at the nano@Stanford labs, supported by the National Science Foundation under award ECCS-2026822.

Datasets and data analysis code are provisioned at `https://doi.org/10.5281/zenodo.5826196`. The simulation package is available at `https://github.com/itrosen/hall-solver`.

[1] A. J. Bestwick, E. J. Fox, X. Kou, L. Pan, K. L. Wang, and D. Goldhaber-Gordon, Phys. Rev. Lett. **114**, 187201 (2015).

[2] C.-Z. Chang, W. Zhao, D. Y. Kim, H. Zhang, B. A. Assaf, D. Heiman, S.-C. Zhang, C. Liu, M. H. W. Chan, and J. S. Moodera, Nat. Mater. **14**, 473 (2015).

[3] E. J. Fox, I. T. Rosen, Y. Yang, G. R. Jones, R. E. Elmquist, X. Kou, L. Pan, K. L. Wang, and D. Goldhaber-Gordon, Phys. Rev. B **98**, 075145 (2018).

[4] M. Götz, K. M. Fijalkowski, E. Pesel, M. Hartl, S. Schreyeck, M. Winnerlein, S. Grauer, H. Scherer, K. Brunner, C. Gould, *et al.*, Appl. Phys. Lett. **112**, 072102 (2018).

[5] Y. Okazaki, T. Oe, M. Kawamura, R. Yoshimi, S. Nakamura, S. Takada, M. Mogi, K. S. Takahashi, A. Tsukazaki, M. Kawasaki, *et al.*, Appl. Phys. Lett. **116**, 143101 (2020).

[6] Y. Okazaki, T. Oe, M. Kawamura, R. Yoshimi, S. Nakamura, S. Takada, M. Mogi, K. S. Takahashi, A. Tsukaxaki, M. Kawasaki, Y. Tokura, and N.-H. Kaneko, Nat. Phys. doi:10.1038/s41567-021-01424-8 (2021).

[7] C.-X. Liu, X.-L. Qi, X. Dai, Z. Fang, and S.-C. Zhang, Phys. Rev. Lett. **101**, 146802 (2008).

[8] R. Yu, W. Zhang, H.-J. Zhang, S.-C. Zhang, X. Dai, and Z. Fang, science **329**, 61 (2010).

[9] M. Allen, Y. Cui, E. Yue Ma, M. Mogi, M. Kawamura, I. C. Fulga, D. Goldhaber-Gordon, Y. Tokura, and Z.-X. Shen, Proc. Natl. Acad. Sci. **116**, 14511 (2019).

[10] J. Wang, B. Lian, H. Zhang, and S.-C. Zhang, Phys. Rev. Lett. **111**, 086803 (2013).

[11] X. Kou, S.-T. Guo, Y. Fan, L. Pan, M. Lang, Y. Jiang, Q. Shao, T. Nie, K. Murata, J. Tang, Y. Wang, L. He, T.-K. Lee, W.-L. Lee, and K. L. Wang, Phys. Rev. Lett. **113**, 137201 (2014).

[12] C.-Z. Chang, W. Zhao, D. Y. Kim, P. Wei, J. K. Jain, C. Liu, M. H. W. Chan, and J. S. Moodera, Phys. Rev. Lett. **115**, 057206 (2015).

[13] B. I. Halperin, Phys. Rev. B **25**, 2185 (1982).

[14] M. Büttiker, Phys. Rev. B **38**, 9375 (1988).

[15] L. K. Rodenbach, I. T. Rosen, E. J. Fox, P. Zhang, L. Pan, K. L. Wang, M. A. Kastner, and D. Goldhaber-Gordon, APL Mater. **9**, 081116 (2021).

[16] A. H. MacDonald, T. M. Rice, and W. F. Brinkman, Phys. Rev. B **28**, 3648 (1983).

[17] H. Hirai and S. Komiyama, Physical Review B **49**, 14012 (1994).

[18] S. Komiyama and H. Hirai, Physical Review B **54**, 2067 (1996).

[19] J. Weis and K. Von Klitzing, Philos. Trans. R. Soc. Lond. A **369**, 3954 (2011).

[20] See Supplemental Material, which includes Refs. [32-42].

[21] M. J. Moelter, J. Evans, G. Elliott, and M. Jackson, Am. J. Phys. **66**, 668 (1998).

[22] I. Lee, C. K. Kim, J. Lee, S. J. Billinge, R. Zhong, J. A. Schneeloch, T. Liu, T. Valla, J. M. Tranquada, G. Gu, *et al.*, Proceedings of the National Academy of Sciences **112**, 1316 (2015).

[23] Y. X. Chong, X. Liu, R. Sharma, A. Kostin, G. Gu, K. Fujita, J. S. Davis, and P. O. Sprau, Nano Letters **20**, 8001 (2020).

[24] P. Fontein, J. Kleinen, P. Hendriks, F. Blom, J. Wolter, H. Lochs, F. Driessen, L. Giling, and C. Beenakker, Physical Review B **43**, 12090 (1991).

[25] T. Ando, Physica B: Condensed Matter **201**, 331 (1994).

[26] S. Wiegers, J. Lok, M. Jeuken, U. Zeitler, J. Maan, and M. Henini, Physical Review B **59**, 7323 (1999).

[27] E. Ahlswede, P. Weitz, J. Weis, K. von Klitzing, and K. Eberl, Phys. B: Condens. Matter **298**, 562 (2001).

[28] M. E. Suddards, A. Baumgartner, M. Henini, and C. J. Mellor, New J. Phys. **14**, 083015 (2012).

[29] K. Panos, R. Gerhardts, J. Weis, and K. Von Klitzing, New Journal of Physics **16**, 113071 (2014).

[30] K. M. Fijalkowski, N. Liu, P. Mandal, S. Schreyeck, K. Brunner, C. Gould, and L. W. Molenkamp, Nat. Commun. **12**, 5599 (2021).

[31] G. Ferguson, R. Xiao, A. R. Richardella, D. Low, N. Samarth, and K. C. Nowack, arXiv preprint arXiv:2112.13122 (2021).

[32] W. Van Der Wel, C. Harmans, and J. Mooij, J. Phys. C: Solid State Phys **21**, L171 (1988).

[33] U. Klaß, W. Dietsche, K. von Klitzing, and K. Ploog, Zeitschrift für Physik B Condensed Matter **82**, 351 (1991).

[34] S. Komiyama, Y. Kawaguchi, T. Osada, and Y. Shiraki, Phys. Rev. Lett. **77**, 558 (1996).

[35] B. P. Dolan, Nuc. Phys. B **554**, 487 (1999).

[36] F. Delahaye and B. Jeckelmann, Metrologia **40**, 217 (2003).

[37] J.-H. Chen, C. Jang S. Adam M. S. Fuhrer E. D. Williams, and M. Ishigami, Nat. Phys. **4**, 377-381 (2008).

[38] G. Granger, J. Eisenstein, and J. Reno, Phys. Rev. Lett. **102**, 086803 (2009).

[39] J. Checkelsky, R. Yoshimi, A. Tsukazaki, K. Takahashi, Y. Kozuka, J. Falson, M. Kawasaki, and Y. Tokura, Nat. Phys. **10**, 731 (2014).

[40] E. O. Lachman, A. F. Young, A. Richardella, J. Cuppens, H. Naren, Y. Anahory, A. Y. Meltzer, A. Kandala, S. Kempinger, Y. Myasoedov, *et al.*, Science advances **1**, e1500740 (2015).

[41] I. T. Rosen, E. J. Fox, X. Kou, L. Pan, K. L. Wang, and D. Goldhaber-Gordon, npj Quantum Materials **2**, 1 (2017).

[42] W. Wang, Y. Ou, C. Liu, Y. Wang, K. He, Q.-K. Xue, and W. Wu, Nature Physics **14**, 791 (2018).